AIAA JOURNAL
Vol. 31, No. 5, May 1993

Asymptotic Methods for the Prediction of Transonic Wind-Tunnel Wall Interference

N. D. Malmuth*
Rockwell International Science Center, Thousand Oaks, California 91360
H. Jafroudi†
University of Southern California, Los Angeles, California 90089
C. C. Wu‡
University of California, Los Angeles, Los Angeles, California 90024
R. McLachlan§
University of Colorado, Boulder, Colorado 80309
and
J. D. Cole¶
Rensselaer Polytechnic Institute, Troy, New York 12180

Two limiting cases related to transonic wind-tunnel wall interference are considered. The first concerning slender airplanes is briefly treated only as it pertains to the main discussion relating to high aspect ratio configurations. Principal features of the slender airplane case are a three-deck flow structure as well as an area rule for interference. Pressure-specified wall conditions are incorporated by addition of averages and Fourier transforms of the wall pressures that modify the far field that controls the interference. For a high aspect ratio two-deck second case, the interference is driven by the imaging in the Trefftz plane projection of the experimental pressure-specified control surface of the (outer deck) trailing vortex system in the Trefftz plane. This gives a downwash correction to a near-field nonlinear lifting line (inner deck) flow. Slightly subsonic freestream conditions give a spikelike interference flowfield due to the interference-induced shock movement for both limiting cases. Approaches integrating the asymptotics with measurement to augment wall interference assessment/correction procedures are outlined.

I. Introduction

FOR the foreseeable future, the wind tunnel will continue to be a vital tool in the development of atmospheric vehicles. In the application of data from such facilities to obtain aircraft performance predictions, wall effects must be accounted for. Procedures to treat subsonic wall interference have received considerable attention. A view of existing technology for this speed regime can be obtained from Refs. 1–3. By contrast, the methodology for the transonic case is much less developed since it gives rise to a particularly difficult nonlinear, mixed-flow environment. Current approaches are exemplified by Refs. 4–6.

In addition to the utility of large-scale computationally intensive methods for transonic wall correction prediction, approaches that can reduce the number of input parameters necessary to compute the correction, shed light on the physics of the wall interference phenomena, simplify the necessary computations, and apply to three dimensions as well as unsteady flows are needed. Asymptotic procedures such as those described in Refs. 7–12 provide such advantages. Furthermore, such techniques can stimulate valuable interactions with the other methods previously mentioned to suggest possible improvements, as well as derive beneficial features from them.

This article summarizes our investigation of combined asymptotic and numerical methods for predicting wall interference. Our theories for slender airplane configurations and high aspect ratio wings will be outlined as well as computational methods to determine the interference flows for these limiting cases. In addition, other approaches will be described

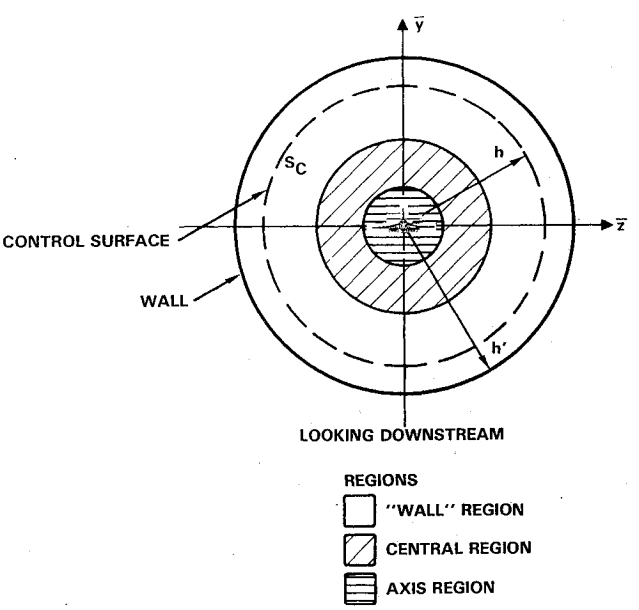

Fig. 1 Slender body within control surface in tunnel.

Presented as Paper 91-1712 at the AIAA 22nd Fluid Dynamics, Plasma Dynamics, and Lasers Conference, Honolulu, HI, June 24–26, 1991; received July 22, 1991; revision received Dec. 23, 1992; accepted for publication Dec. 24, 1992.

*Member of Technical Staff, Computational Fluid Dynamics.
†Research Associate, Aerospace Engineering.
‡Research Physicist, Department of Physics.
§Instructor, Applied Mathematics Department.
¶Professor, Department of Mathematical Sciences.

in which the asymptotics can be integrated with experimental measurements to improve wall interference assessment/correction (WIAC) procedures.

II. Analyses

For both the slender body and high aspect ratio cases, the wall interference is obtained by a systematic asymptotic expansion procedure. Each is represented by a secondary approximation within a Karman-Guderley (KG) transonic small disturbance theory framework. In what follows, the asymptotic structure for the two limits and the formulation of the boundary value problems for the interference perturbation potential are outlined.

Slender Configurations

Figure 1 shows a schematic of a slender airplane of characteristic thickness ratio δ and incidence α within a circular wind tunnel. The quantities h and h' represent radii of "pressure-specified interface" and wall cylinders, respectively. The h interface surface has been introduced to provide experimental pressure data to bypass difficult simulation of ventilated wall boundary conditions.

A double limit consisting of the transonic small disturbance slender body theory (TSDST) described in Ref. 13 and large tunnel radius in units of the body length h in Refs. 11, 12, and 14 gives the three-deck structure shown. In the horizontally shaded "axis" region, crossflow gradients dominate, and the flow is nearly harmonic in crossflow planes. In the slant-shaded "central" zone, relaxation to an axisymmetric nonlinear TSDST environment has occurred. This leads to the equivalence rule given in Ref. 15 and elsewhere for the free field (no walls present) flow. TSDST in the central region is formulated within a distinguished asymptotic limit involving δ, α, and the freestream Mach number M_∞ and leads to the axisymmetric KG equation for the perturbation potential ϕ.

For $H \equiv h\delta \to \infty$, as $\delta \to 0$ the walls linearly and weakly perturb the central region flow. If the walls are axially symmetric, then Refs. 11, 12, 14, and 16 demonstrate that an area rule for wall interference holds in which the interaction of an asymmetric body with walls is the same as its equivalent body of revolution. This interaction is computed from solution of a boundary value problem of the wall correction ϕ_1 to the basic free field flow perturbation potential ϕ_0 whose equation of motion is linear and of mixed type with variable discontinuous coefficients. It is similar to an equation to be shown for the high aspect ratio problem. For slender bodies, boundary conditions for this "variational" equation are obtained from matching with the axis region and a wall region (unshaded zone in Fig. 1) where the approximation of small perturbations of the central region becomes nonuniform due to the $\mathcal{O}(1)$ wall boundary conditions. This wall region is governed by the Prandtl-Glauert equation and the body appears as an imaged multipole for free jet and solid walls. An inner limit of the wall region provides far-field boundary conditions for the variational equation of the central region interference flow. More general pressure-specified wall boundary conditions introduce Fourier transforms and averages of the wall pressure distribution into the far-field boundary conditions. Involved matching procedures to establish this result are detailed in Ref. 12. Numerical procedures and associated issues in solving boundary value problems of this type will be discussed for the high aspect ratio theory in what follows.

High Aspect Ratio Theory

A high aspect ratio wing is shown schematically in Fig. 2 as confined within a cylindrical pressure-specified interface. In contrast to the slender body case, the effect of the lift interference is more significant. Moreover, only two decks are in the flow. One of these is the classical "strip theory" inner (near-field) region of lifting line theory in which each span station of the wing is in a two-dimensional flow independent of the others. As in the slender case, the basic flow is assumed to be given by a KG model, which differentiates it from the classical Prandtl lifting line theory for incompressible flow. For slightly subsonic freestream conditions, the outer (far-field) region structure is that of a lifting line with a trailing vortex sheet in the Prandtl-Glauert (PG) subsonic linear regime. Downwash from this vortex assemblage changes the "geometric" wing incidence. Cook and Cole[17] obtained this correction by matching for the free field problem. Small[18] computed the solution of this problem for the case of similar wing sections. Proper matching conditions for the interference case considered here were obtained from an integral equation based on Green's theorem using a special kernel involving a source reflected in a free jet cylindrical boundary. The Appendix gives further information on these developments. Pressure boundary conditions are incorporated into the model by a superposition procedure detailed in Ref. 12. For the latter, only the first few angular harmonics of Fourier means are important as well as the streamwise variations near the wing, in an asymptotic limit of span and wall height tending to infinity at the same rate. Matching, using the asymptotic solution of the nonlinear integral equation, gives the induced downwash on the loaded line. The reflection effect arises naturally with use of the Green's function and can be interpreted to be phenomenologically the same as that for incompressible flow, i.e., inversion of the vortex system projection in the Trefftz plane into the wall/interface projection. Nonlinear corrections can be obtained systematically using this method.

On implementing these ideas, the variational equation for the wall interference potential ϕ_1 is similar to that for slender bodies. This is a linear variational equation of mixed type whose variable discontinuous coefficients depend on the KG basic free field flow disturbance potential ϕ_0. Asymptotic developments leading to this structure are detailed in Ref. 12 and lead to the following boundary value problem for ϕ_1 for "classical" free jet and solid wall boundary conditions:

$$L[\phi_1] \equiv [K - (\gamma+1)\phi_{0_x}]\,\phi_{1_{xx}} - (\gamma+1)\phi_{0_x}\phi_{1_x} + \phi_{1_{\tilde{y}\tilde{y}}} = 0 \quad \text{(1a)}$$

$$\phi_{1_{\tilde{y}}}(x, 0) = 0; \qquad \phi_1 \to -\tilde{y}[d(z) + w(z)]$$

$$- [\Gamma_1(z)/2\pi]\theta + \cdots + \qquad \text{as } r \to \infty$$

$$[\phi_1]_{\text{wake}} = \Gamma_1(z) \equiv [\phi_1]_{\text{te}} \quad \text{(1b)}$$

where subscript te indicates trailing edge. Here, $d(z)$ and $w(z)$ are crucial functions controlling the size of the aspect ratio and wind-tunnel corrections, respectively. They are given by the integrals

$$d(z) = \frac{1}{4\pi} \int_{-1}^{1} \frac{\Gamma_0'(\xi)}{z - \xi}\, d\xi \quad \text{(2a)}$$

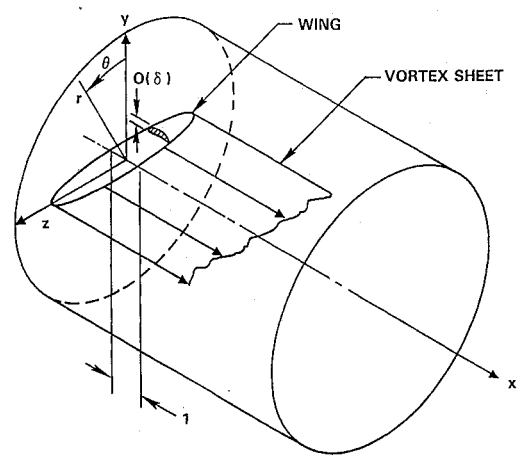

Fig. 2 Confined high aspect ratio wing.

($\oint$ is the principal value integral)

$$w(z) = \pm\frac{\mu^2}{4\pi}\oint_{-1}^{1}\frac{\Gamma_0(\xi)}{(z\xi-\mu^2)^2}\,d\xi \qquad (2b)$$

The function $\Gamma_0(z)$ is the spanwise circulation distribution along the wing in the free field basic flow. In Eq. (2b), the quantity $w(z)$ was obtained from the previously indicated integral equation far-field analysis detailed in Ref. 12, the (+) and (−) apply to free jet and closed wall test sections, respectively, and μ is the the test section width in units of the wing span. Some aspects of the derivation are indicated for free jet wall boundary conditions in the Appendix, which uses the control volume shown in Fig. 3.

Details of the special numerical methods needed to solve the boundary value problem given by Eqs. (1) and its analog for the slender body wall interference case are contained in Refs. 12, 14, and 16, which are generalizations of methods used by Small.[18] Special issues associated with the mixed type structure of this equation and its relation to the Lavrentef-Bitsatze models for transonic shock formation are discussed therein as well as numerical issues concerning the fitting of interference-induced perturbations of shocks captured in the zeroth order KG free field basic flow. Other topics associated with appropriate numerical algorithms are regularization of the far field and other singularities by incorporating asymptotics information into difference and iteration procedures, especially those involving the high aspect ratio wall interference circulation correction. Convergence acceleration methods developed by Hafez and Cheng[19] are particularly useful in this connection.

Asymptotics Integrated with Measurement Methods

The asymptotic formulations outlined in the previous two sections can be exploited to simplify WIAC procedures such as those given in Ref. 20. For nearly slender airplanes, additional measurements of the rate of decay of the radial velocity component or pressure field in the outer part of the logarithmic axis layer described previously give the effective equivalent "soft" body shape as contrasted to the actual "hard" geometry. This measurement is an indication, at least in part, of the thickening effect of the viscous boundary layer. With this, and either the large H theory described earlier or its $H = \mathcal{O}(1)$ counterpart (which could include classical or interfacial pressure boundary conditions), an assessment of the interference or an extrapolation to the free field can be made.

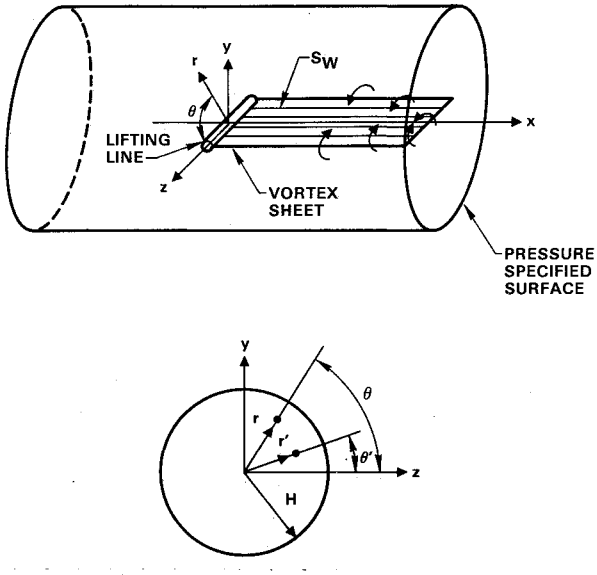

Fig. 3 Far-field flow configuration showing lifting line and vortex sheet.

For high aspect ratio configurations, downwash or other measurements can be used to establish a soft circulation distribution using the relation

$$w = -\frac{1}{4\pi}\oint_{-1}^{1}\gamma'(\zeta)\left\{\frac{1}{z-\zeta}+\frac{\mu^2}{z(z\zeta-\mu)}\right\}d\zeta \qquad (3)$$

In Eq. (3), as well as the discussion associated with Eq. (2b), additional terms can be inserted to account for pressure interface measurements. These corrections, detailed in Ref. 12, are omitted to simplify the discussion.

One asymptotics integrated with measurement (AIM) method based on Eq. (3) evaluates the left-hand side from wake downwash measurements. The function $\Gamma_0(z)$ is then obtained by inverting this integral equation. This can be done on a microcomputer. Extrapolation to the free field is then easily accomplished by using $\Gamma_0(z)$ in Eq. (3) with the wall reflection second term in the braces omitted. This establishes the free field finite span induced incidence correction to the geometric angle of attack. Variants of this approach use deconvolutions based on the high aspect ratio asymptotics described previously as well as other types of measurements.

III. Results

References 12, 14, and 16 contain results for the slender body case. These calculations show a spikelike interference pressure field as well as a change of interference drag to thrust as the Mach number approaches unity and show the intrinsic similitudes of the asymptotic theory which is consistent with those obtained by Goethert[21] using nonasymptotic procedures. The spikelike detail which diffuses with decreasing Mach number is also obtained for high aspect ratios since it is due to the translation of the shock from its free field position. Since the boundary conditions (obtained from asymptotic matching) depend only on the streamwise area progression rather than the cross-sectional shape of the body, an equivalence rule holds that states that the interference flow for asymmetric bodies is identical to those for their equivalent bodies of revolution in TSDST, providing $H = \mathcal{O}(1)$. Also indicated in Refs. 12, 14, and 16 is the resemblance of the pressure distribution away from the spike with that obtained by Malmuth[22] for incompressible flow. Another outgrowth of our analyses of these slender body flows is the shock position invariance law reported in Ref. 23.

For high aspect ratio wings, free jet boundary conditions as well as pressure interface conditions such as

$$C_{P_I} = \epsilon_2 e^{-|x|}\mathrm{sgn}(x)\{1+\epsilon_1\cos\theta\}, \qquad -\infty \le x \le \infty \qquad (4)$$

having certain qualitative features of near-wall pressure distributions were considered, where C_{P_I} is the interfacial pressure

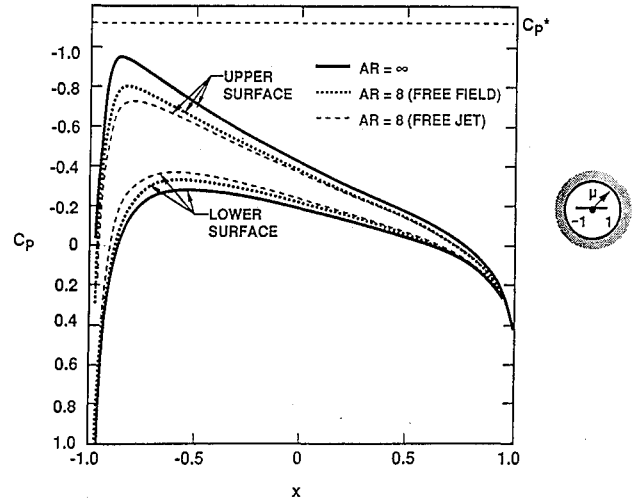

Fig. 4 Chordwise pressures on NACA 0012 wing, $M_\infty = 0.63$.

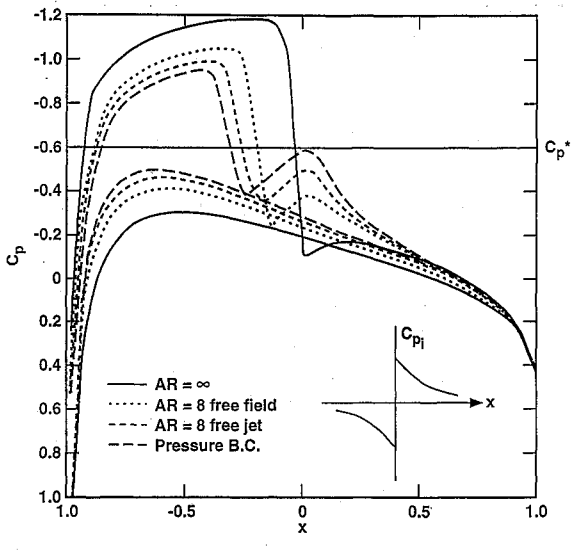

Fig. 5 Chordwise pressures on NACA 0012 wing, $M_\infty = 0.75$, $\epsilon_1 = \epsilon_2 = 0.2$ in Eq. (4) for C_{P_I}.

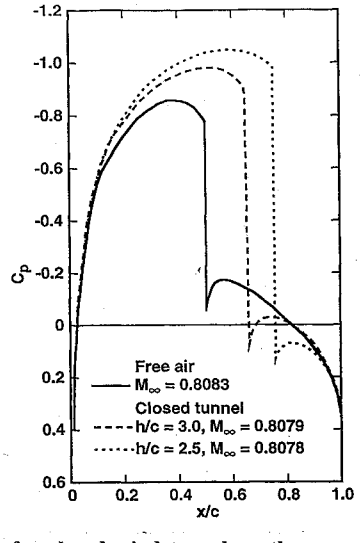

Fig. 6 Effect of a closed wind tunnel on the pressure distribution over a NACA 0012 airfoil from Ref. 26.

distribution; ϵ_1 and ϵ_2 are constants set to the value 0.2 for the calculations; and $\text{sgn}(x) = 1$ for $x > 0$ and -1 for $x < 0$. In Fig. 4, results for an aspect ratio 8 elliptic planform having a NACA 0012 airfoil section are presented. The freestream Mach number M_∞ is 0.63 and the incidence $\alpha = 2$ deg for this subcritical case. Effects of finite span and free jet wall interference on the chordwise pressures show the reduction of lift from both phenomena. Corresponding supercritical results for $M_\infty = 0.75$ at the same angle of attack are shown in Fig. 5. The upstream movement of the shock is associated with the loss of lift that also occurs at this higher Mach number. Such behavior is consistent with qualitative arguments concerning the fact that for proper imaging in the free jet boundary, the image vortex system outboard of a wingtip has the same sense as that around the wingtip. Therefore, this adds to the increased downwash associated with finite aspect ratio and reduces the angle of attack further. The assumed interface pressure gives the same effect in this example.

Figure 5 shows an increase in the rate of re-expansion immediately downstream of the shock when the latter is weakened. This somewhat counterintuitive behavior can be understood in terms of the singularity of transonic small disturbance theory discussed in Ref. 13. The trends in Fig. 5 are supported by experiments and other calculations and are discussed more fully in Ref. 12. The relevance of the experiments is that if the Reynolds number is sufficiently high, the postshock expansion resembles that obtained from the inviscid predictions described in this paper. (Smaller Reynolds numbers will result in postshock boundary-layer separation and are not germane to this discussion.)

Figure 6, taken from Ref. 24, further confirms that weakening the shock exaggerates the re-expansion C_p blip. This behavior has been analyzed in Refs. 13, 25, and 26. Inviscidly, the re-expansion detail represents a logarithmic singularity immediately downstream of the point where the shock strikes the airfoil. If x denotes the distance in the freestream direction measured from the shock impingement point, the b subscript represents conditions immediately behind the shock on the airfoil, M_∞ is the freestream Mach number, δ is the airfoil thickness ratio, $K = (1 - M_\infty^2)/\delta^{2/3}$, and u is the perturbation velocity in the x direction, then if

$$w = (\gamma + 1)u - K \tag{5}$$

the local behavior of the pressure coefficient C_p immediately downstream of the impingement point is given by

$$C_p = C_{p_b} + Ax\ell n(x) \cdots \tag{6}$$

where A is the strength of the singularity given by

$$A = -\frac{8F''(\tilde{x}_0)\delta^{2/3}}{\pi\sqrt{-w_b}} \tag{7}$$

In Eq. (7), $F''(\tilde{x}_0)$ is proportional to the curvature, and $\tilde{x}_0$ represents the x coordinate of the impingement point, measured from the nose. The quantity w_b is proportional to the Mach number jump across the shock. Weakening the shock reduces w_b, increasing the re-expansion singularity strength A. For a NACA 0012 airfoil as well as other profiles, the weakened shock moves upstream and the magnitude of $F''(\tilde{x}_0)$ increases from its downstream value. This has a compounding effect on the increase in A. Data from other profiles confirm this, but obviously it is an airfoil shape-dependent phenomenon.

As an additional verification of these trends, Fig. 7 indicates a comparison of the singularity intensity A from our Mach 0.75 elliptic wing case for free field and pressure boundary conditions (circled points). Also shown are results from Ref. 24 (square points derived from Fig. 6). They correspond to a NACA 0012 airfoil two-dimensional flow in the free field as well as between solid walls for the height to chord ratios shown in Fig. 6. The quantity A was determined from the numerical solution by a least squares fit of the solution using Eq. (6) as the model to fit the solutions. The integral equation method used in Ref. 24 simulates the shock as an instanta-

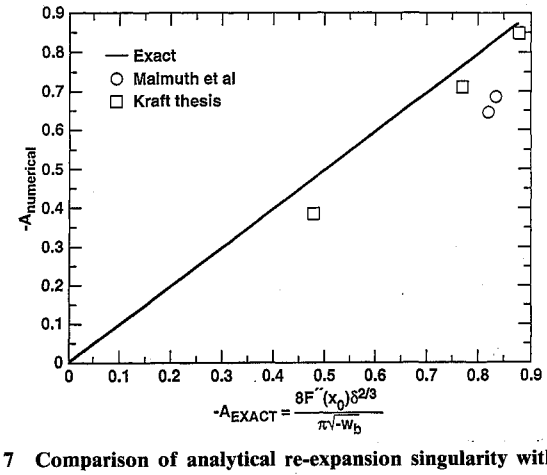

Fig. 7 Comparison of analytical re-expansion singularity with that from numerical solutions.

neous discontinuity, whereas the finite difference solution needs a few points to resolve the shock. These aspects as well as the shock fitting process used in the wall interference perturbation solution are factors affecting the comparison shown. Another is errors committed in digitizing the data near the impingement point. In this connection, at least four points were used for the least squares fit. Although these considerations lead to some minor discrepancies, there is a good correspondence between the numerically determined acceleration of the flow and the local asymptotic estimate.

In addition to the high aspect ratio cases shown, nonsimilar wings have been analyzed. A normalizing transformation that simplifies the computational problem has been discovered. Details of this transformation are discussed in Ref. 12. An important result of the analysis is that with the renormalizations, the calculation can be reduced to the similar section calculation with the exception that the term $\phi_{0_x}\phi_{1_{xx}}$ in Eq. (1a) is no longer computed at $z = 0$. In addition, the quantities d and w are used parametrically at each span station from a knowledge of $\Gamma_0(z)$, the spanwise loading of the zeroth-order problem. This corresponds to a kind of strip theory. To obtain Γ_0, the semispan wing is divided into n span stations, and the zeroth-order (KG) problem detailed in Ref. 12 is solved at each span. For the results to be presented, n was selected to be 5. Depending on the planform, some investigation is required to determine if this value provides a good enough approximation of the spanwise loading to obtain the ϕ_1 variational solution accurately.

Chordwise pressure distributions on the swept wing (wing A) configuration of Ref. 27 were computed at various angles of attack α and Mach number M. To achieve rapid convergence, the streamwise grid was clustered near the blunt leading edge. To demonstrate a typical calculation, Figs. 8 and 9 show the effect of wall interference and finite span corrections on the chordwise pressures of wing A at nearly midspan and at two angles of attack. The largest corrections appear to be near the shock at $\alpha = 0$ deg. By contrast, the more supercritical case corresponding to $\alpha = 1$ deg shows a greater extent of the

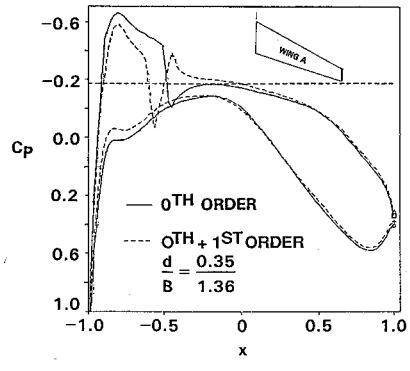

Fig. 8 Zeroth- and first-order chordwise pressure distributions on wing A, $\eta = 0.45$, $M = 0.76$, $\alpha = 0$ deg.

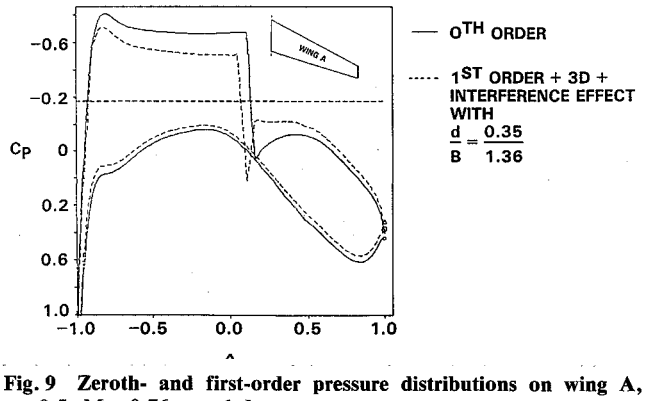

Fig. 9 Zeroth- and first-order pressure distributions on wing A, $\eta = 0.5$, $M = 0.76$, $\alpha = 1$ deg.

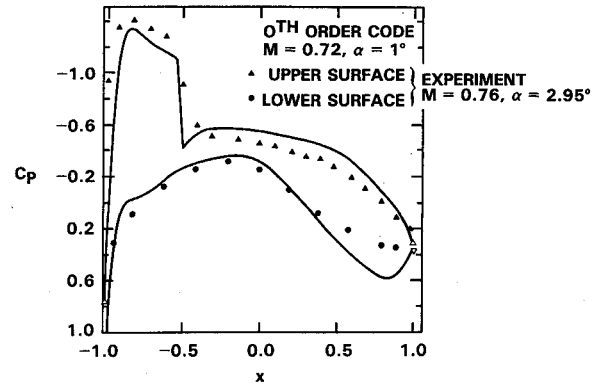

Fig. 10 Comparison of theoretical and experimental chordwise pressures for wing A, $\eta = 0.5$, tested at $M = 0.76$, $\alpha = 2.95$ deg.

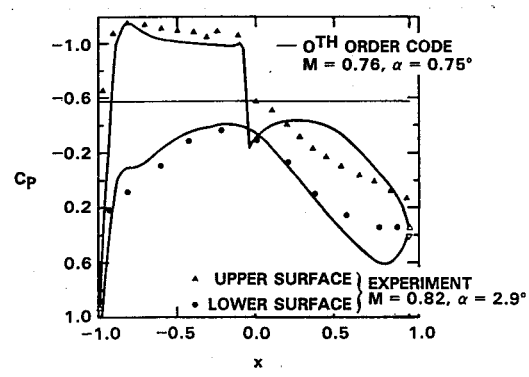

Fig. 11 Comparison of theoretical and experimental chordwise pressures for wing A, $\eta = 0.5$, tested at $M = 0.82$, $\alpha = 2.9$ deg.

corrections. For both incidences, they are most pronounced on the upper wing surface.

In Ref. 13, modifications to the zeroth-order KG boundary value problem are discussed for a yawed wing. The analysis shows that these changes occur in the far field for the three-dimensional first-order perturbation flow and in both the far field and equations of motion for the second-order flow.

The high aspect ratio code is based on a theory not designed for swept wings. This is because the dominant approximation of the inner flow assumes that all spanwise stations are approximately two dimensional. If a discontinuity occurs in the slope of the leading edge, a local three-dimensional flow occurs, nullifying this assumption. Such discontinuities occur at the root apex and tips of swept and other kinds of planforms. More general cases are cranked shapes. Asymptotic procedures are under consideration to treat these corner flows and involve "canonical" numerical problems for the nonlinear flow near the corner. These canonical problems remain the same for planform changes away from the corner.

In spite of this limitation, it was of interest to assess the correctability of the wing A results using the zeroth-order code. Figures 10 and 11 indicate chordwise pressure comparisons of our zeroth-order code with data from Ref. 27. In both figures, the effective tunnel Mach number and angle of attack were modified to match the data. The similarity of the pressure distributions suggests the correctability of the test data. The sweep effect delaying supercriticality is evident and is not reflected in the unswept lifting line forming the basis of the present analysis. In Fig. 10, the influence of shock/boundary-layer interaction is not as great as in Fig. 11.

Results showing effective treatment of viscous effects are reported in Ref. 12. These calculations, which use an interactive boundary model based on Green's lag entrainment method, suggest that the effective increment in K associated with the combined Mach and angle of attack corrections used

in Figs. 10 and 11 can be reduced if viscous interactions effects are systematically incorporated.

In comparisons such as Figs. 10 and 11, what needs to be analyzed are the combined effects of sweepback and viscous interactions on the interference. In Ref. 11, the similarity parameter K was allowed to vary from the zeroth-order flow to the first-order wall interference flow. This flexibility should be investigated with the aim of systemizing the corrections that can be obtained through studies of the type associated with Figs. 10 and 11. The variation of K is expressed in a perturbation form related to the asymptotic expansion of the perturbation potential ϕ. This perturbation gives the flexibility of varying the tunnel Mach number and geometric angle of attack to correct or simulate free field conditions.

IV. Conclusions and Future Work

Asymptotic methods have been used in combination with computational procedures to analyze transonic wall interference. Clearly a substantial advantage inherent in combining these technologies is a reduction in computational effort as well as enhanced insight into the physics, parametric dependencies, scaling, and similitudes. An additional benefit accrues from the asymptotic and numerical approaches augmenting each other's power. On one hand, the asymptotic approach simplifies the numerical problem to be solved. One way this is achieved for the cases considered here is by effectively converting three-dimensional to two-dimensional problems. On the other hand, the numerics solve the analytically intractable aspects. Additional power can be achieved through the integration of experimental measurements with these technologies as exemplified by the two AIM techniques discussed. For slender bodies, the area rule for transonic interference should be exploited in WIAC and other methods to estimate wall effects on drag and pressures in accord with the procedures given previously.

The large wall height slender body theory considered in this paper leads to a triple-deck structure of the interference flow for solid and free jet classical boundary conditions as well as to a means to systematically extrapolate to infinite wall height. It also indicates that the triple-deck structure is altered by a tube vortex with the addition of pressure interface boundary conditions. In the midfield zone of this structure, the spikelike nature of the interference flowfield is a byproduct of the perturbation of the shock position due to the presence of the walls. From the numerical techniques used to analyze this region, the problem of moderate height and noncircular test sections can also be treated. The results given in this paper demonstrate underlying useful similitudes of the interference pressures and drag. This clarifies the parametric dependencies and reduces the number of parameters necessary to describe the transonic interference phenomenon. Experiments are being planned to validate the theories and results in this paper. This will enhance the utility of the asymptotic approach as a basis for "engineering methods" and help determine its parametric validity. Additional extensions of the theory are in progress. These, as well as the validations, will be reported in a future paper. Generalizations in work include an $H = \mathcal{O}(1)$ theory and application of the asymptotic tools to noncircular and variable porosity test sections. The applicability of the equivalence rule for wall interference to the $H = \mathcal{O}(1)$ case will also be explored.

For the slightly subsonic high aspect ratio case with "classical" solid and free jet wall boundary conditions, the interference is driven by the imaging effect of the wall on the projection of the trailing vortex system in the Trefftz plane. In this respect, the far-field interference effect is qualitatively similar to that for incompressible flow. It amounts to a downwash correction to a near-field nonlinear lifting line flow. For free jet boundary conditions, the sense of the imaging is that of the tip relief associated with finite span, and further reduces the lift from (two-dimensional) infinite span levels. Solid wall boundaries reverse this correction. As for the slender body case, pressure interface boundary conditions add induction from a tube vortex coinciding with the interface. For adequate realism, the high aspect ratio methods discussed should be extended to incorporate viscous effects. This appears readily achievable with interacting boundary-layer theory, and such an implementation should further enhance the utility of the tools. This will help validate the theory with previously mentioned planned experiments. General experimental pressure prescribed interface data can be handled by numerical quadratures of the Bessel function kernels in the Ref. 12 slender body far-field expressions using the measured data as convolvers. Some validation of a large height theory against the computations and theory for the finite-height case are given in Refs. 10 and 22.

Appendix

Derivation of the far field for a high aspect ratio wing will be outlined. Referring to Fig. 3, an integral representation for the perturbation potential φ_0 in the far field can be obtained assuming slightly subsonic freestreams, and from coordinate rescaling the resulting Prandtl Glauert (PG) equation becomes Laplace's equation in the rescaled perturbation potential ϕ. Green's theorem gives the following integral equation for ϕ.

$$\phi = I_v + I_{\text{walls}} \tag{A1a}$$

where

$$I_v = \iint_{S_w} [\phi]\left(\frac{\partial G}{\partial n}\right) dS \tag{A1b}$$

$$I_{\text{walls}} = \iint_{\text{walls}} \phi \frac{\partial G}{\partial n} dS \tag{A1c}$$

where G denotes the Green's function, n is the outward drawn normal, S_w is the vortex sheet surface, S_{walls} is the wall surface, and $[\phi]$ signifies the jump in the potential $[\phi]$ across the vortex sheet.

For an open jet wind-tunnel wall boundary condition

$$\phi(x, \mu, \theta) = 0 \tag{A2}$$

corresponding to constant $G(x, \mu, \theta) = I_{\text{walls}} = 0$. The Green's function for this problem is applicable to a generalized far field for pressure-specified boundary conditions on a control surface surrounding the test article.

The appropriate Green's function satisfying a homogeneous Dirichlet condition such as Eq. (A2) on the walls is

$$G = \frac{1}{2\pi\mu^2} \sum_{n=-\infty}^{\infty} \cos n(\theta - \theta') \sum_k \frac{e^{-\lambda_{nk}|x-\xi|} J_n(\lambda_{nk} r) J_n(\lambda_{nk} \rho)}{J_{nk}[J_n'(\lambda_{nk}\mu)]^2} \tag{A3}$$

where

$$\lambda_{nk}\mu = j_{nk}$$

where j_{nk} are the zeros of the J_n Bessel function given by

$$J_n(j_{nk}) = 0 \tag{A4}$$

and

$$\sum_{n=-\infty}^{\infty} (\cdots) = \sum_{n=0}^{\infty} \epsilon_n (\cdots)$$

where $\epsilon_0 = 1$, $\epsilon_n = 2$, and $n > 0$

An alternate representation for G is given by

$$G = -\frac{1}{2\pi^2} \sum_{n=-\infty}^{\infty} \cos n(\theta - \theta') \int_0^{\infty} \cos \xi(x - x') I_n(\xi r') \times \left\{ K_n(\xi r) - \frac{K_n(\xi H) I_n(\xi r)}{I_n(\xi H)} \right\} d\xi \tag{A5}$$

Equation (A5) is in a particularly advantageous form in which the free field component can be separated out in the determination of the wall interference effect. In fact, the first term in the braces leads to the singular part of G, which is a point source in the free field. When this is integrated from $x = 0$ to ∞ and across the span, it gives the free field potential of a loaded line, that is, the dominant approximation of lifting line theory, which is

$$\phi_{LL} = \frac{1}{4\pi}\int_{-1}^{1}\gamma(\zeta)\left\{1+\frac{x}{\sqrt{x^2+y^2+(z-\zeta)^2}}\right\}\left\{\frac{y}{y^2+(z-\zeta)^2}\right\}\mathrm{d}\zeta$$

where $\gamma(\zeta)$ is the spanwise distribution of sectional circulation. This can be shown from the addition theorem for the modified Bessel functions

$$\sum_{n=-\infty}^{\infty}\cos n(\theta-\theta')I_n(\xi r)K_n(\xi r') = K_0(\xi R) \tag{A6a}$$

$$R^2 = r^2 + r'^2 - 2rr'\cos(\theta-\theta') \tag{A6b}$$

and the cosine transform

$$-\frac{1}{2\pi^2}\int_0^{\infty}K_0(\xi R)\cos\xi(x-x')\,\mathrm{d}\xi = -\frac{1}{4\pi\sqrt{R^2+(x-x')^2}} \tag{A7}$$

Thus, the free field potential of a unit intensity isolated source is the right-hand side of Eq. (A7) which by Eqs. (A6) is represented by the first integral in Eq. (A5).

Referring to Fig. 3, I_v can be written as

$$I_v = -\int_{-1}^{1}\gamma(\zeta)\,\mathrm{d}\zeta\int_0^{\infty}\left\{\frac{\partial}{\partial n}G(x^*, y, z^*; \xi, \eta, \zeta)\right\}_{\eta=0}\mathrm{d}\xi \tag{A8}$$

In Eq. (A8), the inner integral represents the potential ϕ_0 of a line doublet parallel to the x axis in the $\eta = 0$ plane and at the span location ζ. Performing the indicated operations,

$$\phi_0 = \int_0^{\infty}\left.\frac{\partial G}{\partial\eta}\right|_{\eta=0}\mathrm{d}\xi$$

$$= \frac{1}{2\pi\mu^2\zeta}\sum_{n=-\infty}^{\infty} n\sin n\left(\theta-\frac{\pi}{2}\right)\sum_k\frac{(2-e^{-\lambda_{nk}x})}{\lambda_{nk}^2[J_n'(\lambda_{nk}\mu)]^2}$$

$$\times J_n(\lambda_{nk}r)\,J_n(\lambda_{nk}\zeta), \qquad \zeta>0 \tag{A9a}$$

$$\phi_0 = \frac{1}{2\pi\mu^2\zeta}\sum_{n=-\infty}^{\infty} n\sin n\left(\theta+\frac{\pi}{2}\right)\sum_k\frac{(2-e^{-\lambda_{nk}x})}{\lambda_{nk}^2[J_n'(\lambda_{nk}\mu)]^2}$$

$$\times J_n(\lambda_{nk}r)\,J_n(\lambda_{nk}\zeta), \qquad \zeta<0 \tag{A9b}$$

Of key interest is the behavior of ϕ_0 and I_v as $x, y \to 0$. This is the essential result sought in determining the downwash on the loaded line and matching with the inner solution. To determine this behavior, ϕ_0 can be further decomposed as follows:

$$\phi_0 = S_1 - S_2, \qquad I_v = \int_{-1}^{1}\gamma(\zeta)\phi_0\,\mathrm{d}\zeta \tag{A10}$$

where, without loss of generality, only $\zeta>0$ will be considered (extension to $\zeta<0$ is trivial), and

$$S_1 \equiv \frac{1}{2\pi\mu^2\zeta}\sum_{n=-\infty}^{\infty} n\sin n\,\bar{\theta}\sum_k\frac{2J_n(\lambda_{nk}r)J_n(\lambda_{nk}\zeta)}{\lambda_{nk}^2[J_n'(\lambda_{nk}\mu)]^2} \tag{A11a}$$

$$S_2 \equiv \frac{1}{2\pi\mu^2\zeta}\sum_{n=-\infty}^{\infty} n\sin n\,\bar{\theta}\sum_k\frac{e^{-\lambda_{nk}x}J_n(\lambda_{nk}r)J_n(\lambda_{nk}\zeta)}{\lambda_{nk}^2[J_n'(\lambda_{nk}\mu)]^2} \tag{A11b}$$

where $\bar{\theta} \equiv \theta - \pi/2$.

Reference 12 evaluates S_1 and S_2 for $x, y \to 0$ to give

$$I_v = \frac{y}{4\pi}\int_{-1}^{1}\gamma(\zeta)\Bigg\{\underbrace{\left[\frac{1}{(z-\zeta)^2+y^2}\right]\left[1+\frac{x}{\sqrt{x^2+y^2+(z-\zeta)^2}}\right]}_{①}$$

$$\pm\underbrace{\frac{\mu^2}{\zeta^2\left[\left(z-\frac{\mu^2}{\zeta}\right)+y^2\right]}}_{②}\Bigg\}\mathrm{d}\zeta + \mathcal{O}(xy) \tag{A12}$$

Equation (A12) provides the dominant inner behavior of the outer solution for the open wall (free jet) case. It contains terms ① which correspond to the free field and ② which are associated with the wall effect. For a solid wall, the sign before ② is negative.

The implication of Eq. (A12) on the matching of the transonic lifting line theory of unconfined high aspect ratio wings given in Ref. 17 is that the horseshoe vortex system, because of its imaging in the walls, modifies the near-field downwash by an amount associated with the term ②. Structurally, the matching elements between the outer and inner solution are otherwise unchanged. Reference 12 details how specified pressure conditions can be incorporated into this far field as an additional term.

Acknowledgments

The major portion of the work described in this paper was supported by the Arnold Engineering Development Center, Air Force Systems Command, U.S. Air Force, under Contracts F40600-82-C-0005 and F40600-84-C-0010.

References

[1]Garner, H. C., Rogers, E. W. E., Acum, W. E. A., and Maskell, E. E., "Subsonic Wind Tunnel Wall Corrections," AGARDograph 109, Oct. 1966.

[2]Pindzola, M., and Lo, C. F., "Boundary Interference at Subsonic Speeds in Tunnels with Ventilated Walls," Arnold Engineering Development Center, AEDC-TR-69-47 (AD 687440), Arnold Air Force Station, TN, May 1979.

[3]Mokry, M., Chan, Y. Y., and Jones, D. V., "Two-Dimensional Wind Tunnel Wall Interference," AGARDograph 281, edited by L. H. Ohman, National Aeronautical Establishment, National Research Council, Ottawa, Canada, Nov. 1983.

[4]Kraft, E. M., Ritter, A., and Laster, M., "Advances at AEDC in Treating Transonic Wind Tunnel Wall Interference," 15th Congress of the International Council of Aeronautical Sciences, ICAS Paper 86-1.6.1, London, UK, Sept. 1986.

[5]Donegan, T. L., Benek, J. A., and Erickson, J. C., "Calculation of Transonic Wall Interference," AIAA 19th Fluid Dynamics, Plasma Dynamics, and Lasers Conference, Honolulu, HI, AIAA Paper 87-1432, June 1987.

[6]Newman, P. A., Hemp, W. B., and Garriz, J. A., "Wall Interference Assessment and Corrections," *Transonic Symposium: Theory, Application and Experiment,* NASA CP-3020, 1988, pp. 817–852.

[7]Lifshits, Y. B., and Fonarev, A. S., "Effect of Flow Boundaries on Parameters of Transonic Flows Around Bodies of Revolution," *Fluid Dynamics,* Vol. 13, 1978, pp. 393–399.

[8]Chan, Y. Y., "A Singular Perturbation Analysis of Two-Dimensional Wind Tunnel Interferences," *Zeitschrift fuer Angewandte Mathematik and Physik,* Vol. 31, 1980, pp. 605–619.

[9]Blynskaya, A. A., and Lifshits, Y. B., "Transonic Flows Around an Airfoil in Wind Tunnels," *Fluid Dynamics,* Vol. 15, 1981, pp. 711–718.

[10]Cole, J. D., Malmuth, N. D., and Ziegler, F. "An Asymptotic Theory of Solid Tunnel Wall Interference," AIAA/ASME 3rd Joint Thermophysics, Fluids, Plasma, and Heat Transfer Conference, St. Louis, MO, AIAA Paper 82-0933, June 1982.

[11]Malmuth, N. D., and Cole, J. D., "Study of Asymptotic Theory of Transonic Wind Tunnel Interference," Final Rept. for Period May 30, 1982–Aug. 30, 1983, Contract F40600-82-C-0005, Arnold Engineering Development Center/DOS Rept. AEDC-TR-84-8, Tulla-

homa, TN, May 1984.

[12]Malmuth, N. D., Wu, C. C., Jafroudi, H., Mclachlan, R., Cole, J. D., and Sahu, R., "Asymptotic Theory of Wind Tunnel Wall Interference," Arnold Engineering Development Center, Final Rept. for Contract F40600-84-C-0010, AEDC-TR-91-24, Arnold Air Force Station, TN, Dec. 1991.

[13]Cole, J. D., and Cook, L. P., *Transonic Aerodynamics,* North-Holland, New York, 1986.

[14]Malmuth, N. D., "Asymptotic Methods for Prediction of Transonic Wind Tunnel Wall Interference," Keynote Lecture—International Conference on Adaptive Wall Wind Tunnel Research and Wall Interference Correction, Xian, Shaanxi, China, June 10–14, 1991.

[15]Oswatitsch, K., and Kuene, F., "Ein Aquivalensatz fur Nichangestellte Fluge Kleiner Spannweite in Schallnaher Stromung," *Zietschrift für Flugwissenshaften,* Vol. 3, No. 2, 1955, pp. 39–46.

[16]Malmuth, N. D., "Some Applications of Combined Asymptotics and Numerics in Fluid Dynamics and Aerodynamics," *Frontiers in Applied Mathematics,* Society of Industrial and Applied Mathematics, Philadelphia, PA, 1993.

[17]Cook, L. P., and Cole, J. D., "Lifting Line Theory for Transonic Flow," *Journal of Applied Mathematics,* Vol. 35, No. 2, 1978, pp. 209–228.

[18]Small, R. D., "Studies in Transonic Flow VI, Calculation of a Transonic Lifting Line Theory," Univ. of California Los Angeles, Rept. UCLA-ENG-7836, Los Angeles, CA, April 1978.

[19]Hafez, M. M., and Cheng, H. K., "Convergence Acceleration of Relaxation Solutions for Transonic Computations," AIAA Paper 75-71, 1975.

[20]Lo, C. F., and Sickles, W. F., "Two-Measured Variable Method for Wall Interference Assessment/Correction," *Transonic Symposium: Theory, Application and Experiment,* NASA CP-3020, 1988, pp. 853–866.

[21]Goethert, B. H., *Transonic Wind Tunnel Testing,* Pergamon, New York, 1961.

[22]Malmuth, N. D., "An Asymptotic Theory of Wind Tunnel Wall Interference on Subsonic Slender Bodies," *Journal of Fluid Mechanics,* Vol. 177, 1987, pp. 19–35.

[23]Cole, J. D., and Malmuth, N. D., "Shock Wave Location on a Slender Transonic Body of Revolution," *Mechanics Research Communications,* Vol. 10, No. 6, 1989, pp. 353–335.

[24]Kraft, E. M., "An Integral Equation Method for Boundary Interference in Perforated-Wall Wind Tunnels at Transonic Speeds," Ph.D. Dissertation, Univ. of Tennessee, Tullahoma, TN, Dec. 1975.

[25]Gadd, G. E., "The Possibility of Normal Shock Waves On a Body With Convex Surfaces in Inviscid Transonic Flow," *Zeitschrift fuer Angewandte Mathematik and Physik,* Vol. 11, 1960, pp. 51–55.

[26]Oswatitsch, K., and Zierep, J., "Das Problem des Senkrechten Stosses an einer gekrümmten Wand," *Zeitschrift fuer Angewandte Mathematik and Physik,* Supplement, 1960, pp. 143–144.

[27]Hinson, B. L., and Burdges, K. P., "Acquisition and Application of Transonic Wing and Far Field Test Data for Three-Dimensional Computational Method Evaluation," Air Force Office of Scientific Research, AFOSR Rept. 80-0421, Washington, DC, March 1980.